DE GRUYTER

Biol. Chem. 2024; 405(11–12): 751–763

Arend Vogt*, Raik Paulat, Daniel Parthier, Verena Just, Michal Szczepek, Patrick Scheerer, Qianzhao Xu, Andreas Möglich, Dietmar Schmitz, Benjamin R. Rost* and Nikolaus Wenger

Simultaneous spectral illumination of microplates for high-throughput optogenetics and photobiology

Abstract: The biophysical characterization and engineering of optogenetic tools and photobiological systems has been hampered by the lack of efficient methods for spectral illumination of microplates for high-throughput analysis of action spectra. Current methods to determine action spectra only allow the sequential spectral illumination of individual wells. Here we present the open-source RainbowCap-system, which combines LEDs and optical filters in a standard 96-well microplate format for simultaneous and spectrally defined illumination. The RainbowCap provides equal photon flux for each wavelength, with the output of the LEDs narrowed by optical bandpass filters. We validated the RainbowCap for photoactivatable G protein-coupled receptors (opto-GPCRs) and enzymes for the control of intracellular downstream signaling. The simultaneous, spectrally defined illumination provides minimal interruption during time-series measurements, while resolving 10 nm differences in the action spectra of optogenetic proteins under identical experimental conditions. The RainbowCap is also suitable for studying the spectral dependence of light-regulated gene expression in bacteria, which requires illumination over several hours. In summary, the RainbowCap provides high-throughput spectral illumination of microplates, while its modular, customizable design allows easy adaptation to a wide range of optogenetic and photobiological applications.

Keywords: action spectra; cyclic mononucleotides; GPCR; photoactivated nucleotidyl cyclases; rhodopsin; signal transduction

Benjamin R. Rost and Nikolaus Wenger contributed equally to this work.

---

*Corresponding authors: Arend Vogt, Department of Neurology with Experimental Neurology, Translational Neuromodulation Group, Charité – Universitätsmedizin Berlin, Corporate Member of Freie Universität Berlin and Humboldt-Universität zu Berlin, D-10117 Berlin, Germany; and Neuroscience Research Center, Charité – Universitätsmedizin Berlin, Corporate Member of Freie Universität Berlin and Humboldt-Universität zu Berlin, D-10117 Berlin, Germany, E-mail: arend.vogt@charite.de. https://orcid.org/0000-0003-0925-0308 (A. Vogt); and **Benjamin R. Rost**, Neuroscience Research Center, Charité – Universitätsmedizin Berlin, Corporate Member of Freie Universität Berlin and Humboldt-Universität zu Berlin, D-10117 Berlin, Germany; and German Center for Neurodegenerative Diseases (DZNE), D-10117 Berlin, Germany, E-mail: benjamin.rost@dzne.de. https://orcid.org/0000-0003-1906-0081 (B.R. Rost)
Raik Paulat and Verena Just, Department of Neurology with Experimental Neurology, Translational Neuromodulation Group, Charité – Universitätsmedizin Berlin, Corporate Member of Freie Universität Berlin and Humboldt-Universität zu Berlin, D-10117 Berlin, Germany; and Faculty of Energy and Information, HTW-Berlin University for Applied Sciences, D-10318 Berlin, Germany, E-mail: raik.paulat@charite.de (R. Paulat), verena.just16@web.de (V. Just). https://orcid.org/0000-0002-1810-6036 (R. Paulat)
Daniel Parthier, Neuroscience Research Center, Charité – Universitätsmedizin Berlin, Corporate Member of Freie Universität Berlin and Humboldt-Universität zu Berlin, D-10117 Berlin, Germany, E-mail: daniel.parthier@charite.de. https://orcid.org/0000-0001-8775-024X
Michal Szczepek and Patrick Scheerer, Institute of Medical Physics and Biophysics, Group Structural Biology of Cellular Signaling, Charité – Universitätsmedizin Berlin, Corporate Member of Freie Universität Berlin and Humboldt-Universität zu Berlin, D-10117 Berlin, Germany, E-mail: michal.szczepek@charite.de (M. Szczepek), patrick.scheerer@charite.de (P. Scheerer). https://orcid.org/0000-0001-5079-6893 (M. Szczepek). https://orcid.org/0000-0001-5028-2075 (P. Scheerer)
Qianzhao Xu and Andreas Möglich, Department of Biochemistry, University of Bayreuth, D-95447 Bayreuth, Germany, E-mail: qianzhaoxu@qq.com (Q. Xu), andreas.moeglich@uni-bayreuth.de (A. Möglich). https://orcid.org/0000-0002-7382-2772 (A. Möglich)
Dietmar Schmitz, Neuroscience Research Center, Charité – Universitätsmedizin Berlin, Corporate Member of Freie Universität Berlin and Humboldt-Universität zu Berlin, D-10117 Berlin, Germany; and German Center for Neurodegenerative Diseases (DZNE), D-10117 Berlin, Germany, E-mail: dietmar.schmitz@charite.de. https://orcid.org/0000-0003-2741-5241
Nikolaus Wenger, Department of Neurology with Experimental Neurology, Translational Neuromodulation Group, Charité – Universitätsmedizin Berlin, Corporate Member of Freie Universität Berlin and Humboldt-Universität zu Berlin, D-10117 Berlin, Germany, E-mail: nikolaus.wenger@charite.de. https://orcid.org/0000-0002-0965-7530

1 Introduction

Gene-expression of ectopic, light-sensitive proteins combined with targeted light delivery allows for precise photocontrol of various cellular functions. The method, commonly termed optogenetics, has developed greatly in the last 20 years and is now broadly applied in various areas of the life sciences (Emiliani et al. 2022; Tan et al. 2022). Optogenetics is also increasingly being explored as part of gene therapy strategies for pathophysiological conditions such as blindness, hearing impairment, cancer and neurodegenerative diseases (Kleinlogel et al. 2020; Malogolovkin et al. 2022; Murphy et al. 2021; Sahel et al. 2021). Essential for the successful application of light-sensitive proteins in heterologous expression systems is the understanding of their biophysical properties. The action spectrum in living cells is particularly relevant, as it indicates which wavelengths activate the photoreceptor and defines peak sensitivity. A precise definition of the action spectra allows reducing light intensities for activation and to minimize side effects such as unintended pre-activation or phototoxicity. In addition, knowledge of the action spectra enables the combination with other optogenetic actuators and fluorescent biosensors with complementary optical properties.

Several methods have been established to determine action spectra. Electrophysiological readouts are ideal for studying light-gated ion channels and light-driven ion pumps (Chow et al. 2010; Klapoetke et al. 2014), because their activity can be measured directly as electrical signal. However, the electrophysiological determination of the action spectra of optogenetic proteins that trigger cell signaling cascades such as light-activated G protein-coupled receptors (opto-GPCRs) and opto-enzymes (Muhlhauser et al. 2017; Spangler and Bruchas 2017) is more challenging. A common strategy for monitoring light-driven signaling mediated by second messengers like cyclic mononucleotides (cAMP or cGMP) is to record the subsequent activation of co-expressed ion channels. The activity of opto-GPCRs or light-activated cyclases can be monitored via the activation of cyclic nucleotide–gated ion channels (CNG), such as the cyclic adenosine monophosphate (cAMP)-gated potassium channel SthK and the cyclic guanosine monophosphate (cGMP)-gated CNG-A2 or BeCNG1 channels (Bernal Sierra et al. 2018; Henss et al. 2022; Scheib et al. 2015). Signaling of $G\alpha_{i/o}$-coupled opto-GPCRs has also been monitored by the activation of G protein-gated inwardly rectifying potassium channels (GIRKs) via the G protein $\beta\gamma$-subunits. This strategy was used for cone opsins, melanopsin (Opn4) and mosquito Opn3 (Mahn et al. 2021; Masseck et al. 2014; Spoida et al. 2016). However, such recordings from single cells are labor-intensive and time-consuming, as individual wavelengths have to be tested sequentially (Spoida et al. 2016). In addition, repetitive illumination with different wavelengths can lead to undefined secondary photoreactions and bleaching effects. High-throughput measurements of action spectra using microplates and plate readers could overcome these limitations. Light-induced changes of cyclic nucleotide levels can be determined by immunoassays (Gao et al. 2015), but these end-point measurements fail to provide information on the signaling dynamics. Fluorescence-based measurements are challenging for studying photo-activated proteins because the fluorescent readout requires repeated light exposure of the cells. In contrast, luminescence-based readouts do not require illumination. These approaches rely on light-emitting luciferases that increase their luminescence in response to an intracellular signal. For example, the Ca^{2+}-signal of the light-activated human melanopsin has been monitored by coexpressing the Ca^{2+}-dependent luciferase aequorin (Bailes and Lucas 2013). The GloSensor assay is based on cyclic nucleotide-dependent luciferases that generate luminescence in response to cAMP or cGMP (Binkowski et al. 2011). This assay can be used for detecting light-triggered alterations of intracellular cAMP- or cGMP levels by opto-GPCRs and opto-enzymes such as photoactivated cyclases and phosphodiesterases (Bailes and Lucas 2013; Gerrard et al. 2018; Mahn et al. 2021; Sugiura et al. 2020; Yoshida et al. 2017). Ballister et al. (2018) developed an elegant extension of the GloSensor assay that simplifies the study of opto-GPCRs with different coupling specificities. This "GsX" assay employs C-terminal chimeras of the $G\alpha_s$ protein, in which the receptor-interacting part is replaced by the C-terminus of different Gα subunits (e.g., $G\alpha_i$, $G\alpha_o$, $G\alpha_t$, $G\alpha_q$). Such chimeric $G\alpha_sX$ subunits displace the endogenous Gα subunits that normally interact with the GPCR, and redirect the GPCR signal into activation of the adenylyl cyclase and thus an increase in cAMP levels (Ballister et al. 2018). The advantage of this assay is that different coupling specificities of GPCRs can be investigated in a single assay. As receptor activation always leads to an increase in the cAMP level, this can be easily quantified with the GloSensor assay. Luminescence-based measurements in combination with the GsX assay are therefore well suited for performing high-throughput experiments on living cells to study opto-GPCR signal transduction in microplates.

For microplates, various illuminations systems with different specifications and complexities have been developed in recent years (Kumar and Khammash 2022). Among these, only one was specifically developed for action spectra (Richter et al. 2015). The light from the color LEDs was transmitted into a plate reader via an optical fiber. While this design enables fully automated illumination protocols, only one well could be illuminated at a time, causing non-simultaneous stimulation and eventually long-time delays in the protocols. This limitation

also applies to the use of built-in light sources of plate readers for fluorescence measurements. In addition, using the unfiltered light from LEDs for stimulation can compromise the determination of the action spectrum, since many LEDs emit light with a Gaussian spectral shape that spans several 10 nm.

We therefore engineered the RainbowCap-system for simultaneous spectral activation and measurement of action spectra in 96-well microplates. Our system is based on color LEDs, with their emission spectra narrowed with optical filters. LED intensities together with the filters were adjusted to provide a uniform photon flux. Light titration experiments can be performed by varying the illumination time. We evaluated the system on two prototypical eukaryotic opsins, bovine rhodopsin and JellyOp, a visual opsin from the box jellyfish *Carybdea rastonii*. For action spectra analysis, we implemented an analytical pipeline that uses Bayesian statistics to fit the Govardovskii template to the experimental values (Gabry et al. 2019; Govardovskii et al. 2000). Experiments with serum-free cell cultures show that the retinal isomers 9-*cis*, 11-*cis*, and 13-*cis* contribute significantly to the spectral properties of JellyOp. Furthermore, we measured action spectra of photoactivated adenylyl- and guanylyl cyclases, and extended the application to the light-controlled gene expression system pDawn-DsRed (Ohlendorf et al. 2012). We demonstrate that the Rainbow-Cap is efficient for the simultaneous spectral illumination of microplates, and that it allows determining quantitative and high-quality spectra of various optogenetic tools.

2 Results

2.1 Engineering of the RainbowCap-system

We considered the following aspects when implementing our illumination device: Preliminary experiments with flashlights and transfected HEK293TN cells indicated that simple commercial 5 mm LEDs are bright enough to activate optogenetic proteins for cell signaling. Moreover, illumination times of a few seconds are sufficient for saturating photostimulation. Therefore, no laser or cooling system is needed. White microplates with opaque bottoms are most efficient for luminescence assays, i.e. illumination must come from above. Figure 1A shows the final design of our spectral illumination system, the RainbowCap, which comprises the illumination plate, a microcontroller, and a power supply. The illumination plate itself consists of two interconnected 3D-printed black subplates (Figure 1B and C, Supplementary Figure 1). The base plate (filter plate) provides slots for optical filters with a diameter of 5 mm. The lateral bracket simplifies handling and serves as a mounting option. The upper plate contains the LEDs (LED plate) and the electrical wiring. Both subplates were designed with protruding edges aligned to the wells, which prevents light scattering into adjacent wells. The electronic and optical details are described in the Methods section and in the Supplementary Figures 2–4.
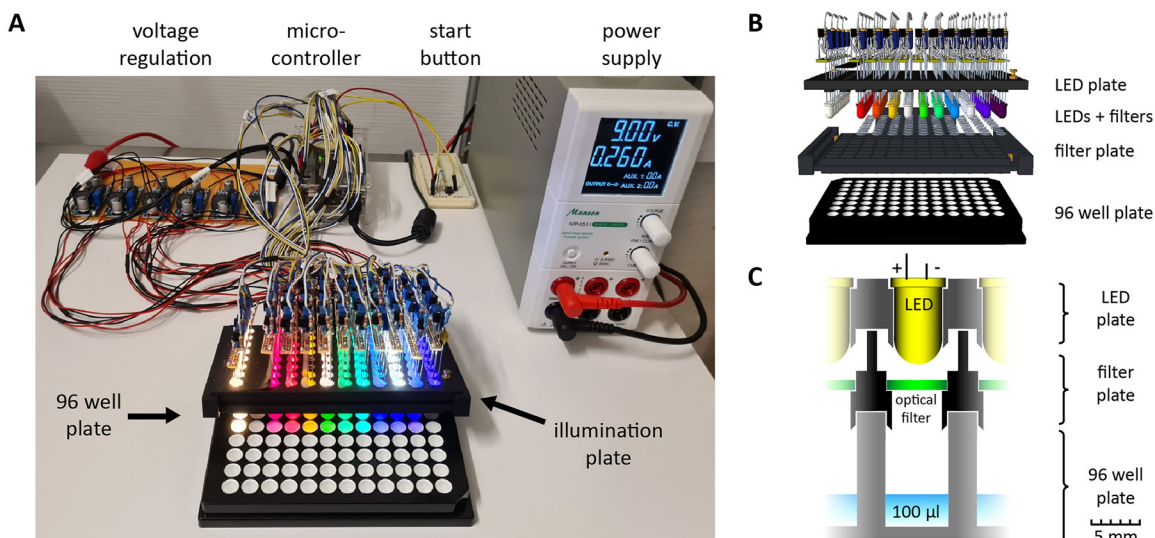

Figure 1: The RainbowCap spectral illumination system for microplates. (A) The components of the RainbowCap. (B) Blow-up scheme illustrating the assembly of the illumination plate aligned to a 96-well plate. The illumination plate consists of a bottom plate that holds the optical filters, and a top plate that holds the LEDs. Both subplates are stably connected with screws. (C) Cross-section of a single well with the illumination plate placed on top.
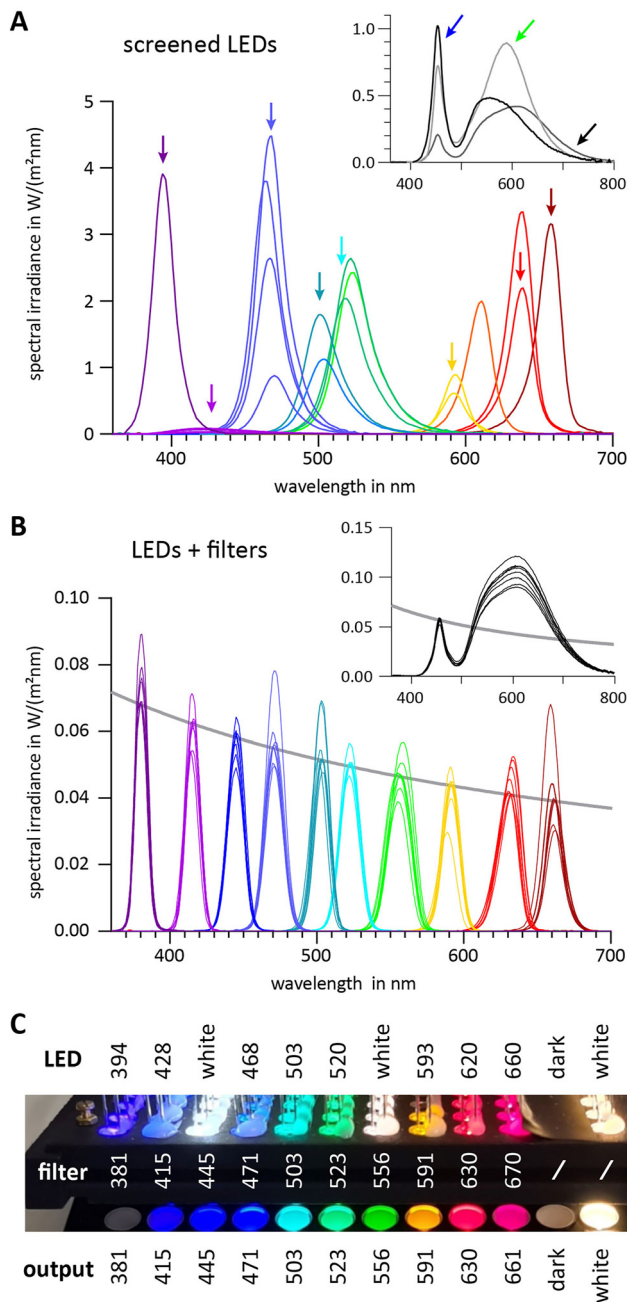
A

B

C

Figure 2: Optimization of the optical components of the RainbowCap for high spectral resolution and uniform photon flux. (A) Spectra and light intensities of 26 LEDs from different manufacturers. All measurements were done with 20 mA current. Light intensities vary and spectral overlaps are observed, while some spectral ranges are barely covered by the LED output. Arrows indicate the LEDs selected for the illumination plate. Inset shows measurements for three white light LEDs. Of these, two LEDs were chosen for the 445 and 556 nm illumination (blue and green arrow, respectively). The black arrow denotes the LED chosen for white light illumination. (B) Spectra and light intensities of individual LEDs after integration into the RainbowCap. Each line represents the spectral output of an individual LED. LED-filter pairs were selected to achieve 10 different colors evenly distributed over the visual spectrum. Electrical currents were adjusted to achieve equal photon flux for all output wavelengths,

The key components of the RainbowCap are the LEDs and optical filters, which we matched and adjusted to achieve a uniform photon flux within the range of 381–661 nm. To this end, we first screened 23 narrow band and 3 "white" LEDs from different suppliers at a constant current of 20 mA and measured their intensities and emission spectra (Figure 2A). Measurements of light spectra and intensities were accomplished with a spectroradiometer and a custom-made adapter that positioned the sensor below the LEDs, thereby replicating the configuration of the microplate (Supplementary Figure 5). LED intensities differed by a factor of >100, and we observed considerable spectral overlaps. We then narrowed the spectral output of the selected LEDs with bandpass filters (Figure 2B and C, Supplementary Figure 4). Using the spectroradiometer adapter setup, the LED-filter pairs were calibrated to provide equal photon flux at each wavelength (1.3×10^{17} photons/m^{2}s). Given the considerable variation in light output among different types of LEDs, we had to drastically reduce the brightness of some LEDs while operating others at maximum output, which set the upper limit for the light output. To fill spectral gaps at 445 and 556 nm, we combined bandpass filters with wide-spectrum ("white light") LEDs. In the illumination configuration, the first 10 columns of the 96-well microplate are each illuminated with a defined light color (Figure 2C). The 11th column is not illuminated and serves as a dark control to detect possible pre-activation or dark activity. The white light LED in the last column serves as a positive control. For this LED, the blue light component was normalized to the uniform photon flux (Figure 2B, inset), but the total intensity integral of the white light LED is significantly larger than that of the other LEDs.

2.2 Measurement of rhodopsin action spectra

We tested the RainbowCap on JellyOp and bovine rhodopsin (bovRho), two well-established opto-GPCRs, using the Glo-Sensor assay as readout (Figure 3A). The JellyOp triggers Gα$_s$ signaling, which has been applied for example to increase the contraction frequency of cardiomyocytes (Bailes et al. 2012; Koyanagi et al. 2008; Makowka et al. 2019). BovRho was the first GPCR for which crystal structures in inactive and active states

indicated by the curved gray line. (C) LED light output before and after passing through the optical filters. Numbers indicate the central wavelength of the bandpass filters and the maximum wavelength (in nm) of the output spectra below the filter. White light LEDs combined with filters were used for 445 and 550 nm. The 381 nm LED output appears dark due to the insensitivity of the camera sensor to UV.
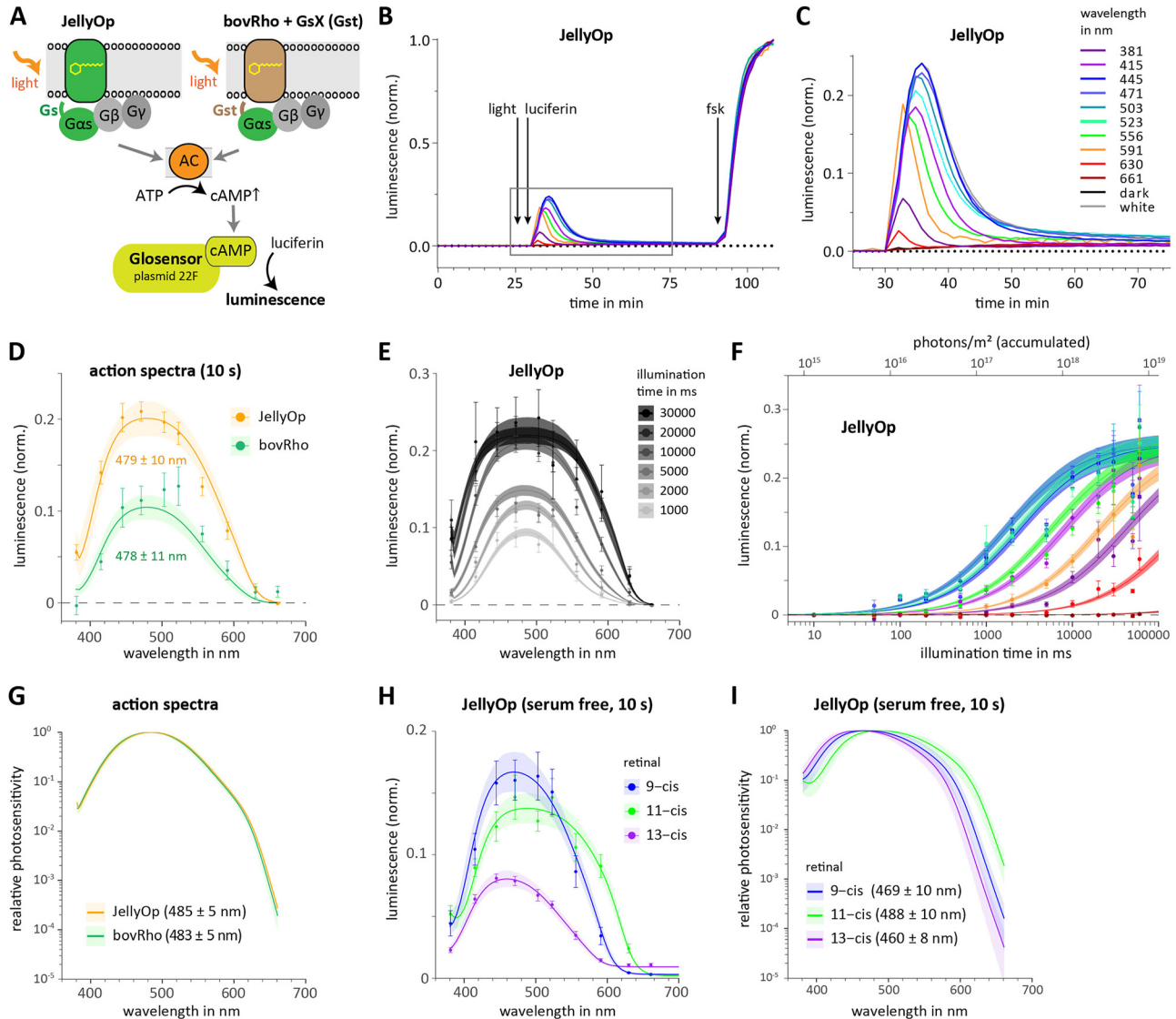
Figure 3: Recording action spectra of opto-GPCRs with the RainbowCap. (A) Scheme illustrating cAMP-dependent GloSensor activation by opto-GPCRs. Jellyfish rhodopsin (JellyOp) directly stimulates the endogenous adenylyl cyclase (AC) via Gα$_s$, which increases intracellular cAMP levels. Bovine rhodopsin (bovRho) natively couples to Gα$_t$ (transducin). Coexpression of bovRho with a chimeric Gα$_{st}$ protein redirects the signal into stimulation of the adenylyl cyclase. (B) Light-induced cAMP increase by illuminating JellyOp-expressing cells at different wavelengths for 10 s. Luciferin was added immediately after illumination. Light-independent stimulation of the adenylyl cyclase with 10 μM forskolin (fsk) allows normalization of the measurements. (C) Inset showing light-triggered response from B. (D) Action spectra of JellyOp and bovRho after 10 s illumination. (E) Light titration of JellyOp. Data as in D but with additional illumination times. (F) Dose response curves of JellyOp to determine the relative photosensitivity for each wavelength. (G) Action spectra based on the relative photo-sensitivities of JellyOp and bovRho. (H) Action spectra of JellyOp 1–2 h after reconstitution with 1 μM of freshly purified retinal isomers. Cells were illuminated for 10 s and cultured in serum-free medium. (I) Normalized spectra of JellyOp with data from subfigure H. Data points are indicated as mean ± SEM (*n*-values in Supplementary Figure 10). Curve fits are performed with statistic modeling and the rhodopsin nomogram. The errors of λ$_{max}$ and curve fits indicate the range in which the data are within a probability of 95 %.

were available (Choe et al. 2011; Palczewski et al. 2000; Park et al. 2008; Scheerer et al. 2008), and rod rhodopsins from bovine and rat were used in pioneering optogenetic experiments (Khorana et al. 1988; Li et al. 2005). It provides scotopic low-light vision and triggers Gα$_t$ (transducin) coupled signaling *in vivo* and *in vitro,* but Gα$_{i/o}$ signaling was also observed *in vitro* (Ballister et al. 2018; Hofmann et al. 2009; Kanaho et al.

1984; Terakita et al. 2002). However, by using the GsX assay (including the C-terminus of Gα$_t$ in chimeric Gα$_s$), signaling of bovRho can be redirected into Gα$_s$ signaling and a cAMP increase (Ballister et al. 2018).

As outlined above, the major advantages of the GloSensor assay are its compatibility with living cells and that no excitation light is required for the readout. A drawback

is that the substrate luciferin is fluorescent, with excitation around 380 nm and emission in the range of 480–640 nm (Supplementary Figure 6A). If the luciferin fluorescence evoked by light of short wavelength excites rhodopsins, this could lead to a distortion of the action spectrum as observed with bovRho (Supplementary Figure 6C–F). We therefore decided to use a measurement workflow with spectral illumination preceding the luciferin application (Figure 3B, Supplementary Figure 6B and C). After equilibrating the plate in the reader and recording of shot noise, the cells were illuminated with the RainbowCap and the plate was quickly placed back into the plate reader. Immediately afterwards, luciferin was added by automatic injection by the reader. We kept the plate outside the reader for the shortest possible duration, as cooling of the plate results in a temperature artifact that occurs already after 1 min (Supplementary Figure 7). Upon illumination for 10 s and luciferin application, the signal of JellyOp reached a maximum after 3 min and returned to baseline after 20 min (Figure 3B and C). At the end of the measurement, 10 μM forskolin (fsk), a direct stimulator of the endogenous adenylyl cyclase, was added per injection. Fsk served as a light-independent control for normalization. For the first tests we cultured cells in serum supplemented with 1 μM all-*trans* retinal upon cultivation in microplates, resulting in a retinal-isomer mixture after hours in the dark (Brueggemann and Sullivan 2002; Deval and Singh 1988).

In order to determine the spectral activity, we implemented a statistical model (Bayesian workflow) in combination with a template for rhodopsin spectra (Gabry et al. 2019; Govardovskii et al. 2000). The Govardovskii template was originally developed for fitting absorption spectra of animal rhodopsins. The statistical method simulates the spectrum multiple times and allows the incorporation of data from different experimental settings (see Supplementary Materials for details). We found greatly improved fits when relaxing the parameters of the nomogram for calculating the action spectra based on the Glosensor assay. Figure 3D shows the resulting action spectra for JellyOp with λ_{max} 479 ± 10 nm and bovRho with λ_{max} 478 ± 11 nm obtained just from a non-saturating 10 s illumination (error range indicates 95 % probability).

To obtain a more precise estimation of the activity spectrum, we applied different light dosages to evaluate the relative spectral sensitivity of JellyOp and bovRho over a wide dynamic range. The RainbowCap offers four adjustable illumination times per plate, allowing experiments with four different photon-dosages (Supplementary Figure 8). For more illumination times, we compared the fsk-normalized values from different plates. The resulting action spectra and irradiance-response curves for JellyOp are shown in Figure 3E and F (bovRho in Supplementary Figure 6G and H). For orange

and red light, we could not achieve saturation with 60 s illumination, thus we extrapolated the irradiance-response relations for these wavelengths (see Supplementary Materials). The resulting relative photosensitivity spectra based on the half-maximal light intensities are shown in Figure 3G. By applying the statistical model and the Govardovskii template, we obtained a λ_{max} of 485 ± 5 nm for JellyOp and 483 ± 5 nm for bovRho. These values are red-shifted by about 5–6 nm compared to the activity peaks obtained by 10 s illumination alone, probably reflecting a better determination of the red light activation of the opsins with longer illumination times.

Next, we investigated how specific retinal isomers contribute to the spectral properties of JellyOp. For this, we established serum-free HEK293TN cultures, which we supplemented with the specific retinal isomers 1–2 h before illumination (Figure 3H and I). We observed highest activity of JellyOp for 9-*cis* retinal (469 ± 10 nm), followed by 11-*cis* retinal (λ_{max} of 488 ± 10 nm). JellyOp also showed activity after reconstitution with 13-*cis* retinal (λ_{max} of 460 ± 8 nm), but with less efficiency and significant dark activity. Of note, we found that adding all-*trans* retinal to JellyOp induces activity in the dark, which slowly decays over several hours (Supplementary Figure 9). The effect is only observed when cells are grown in absence of any retinal (compare to Supplementary Figure 6B). Illumination with white light abolishes the dark activity. In contrast, addition of 11-*cis* does not elicit activity *per se*, but enables a robust light inducible response. The dark activity can be explained by all-*trans* retinal representing the chromophore of the active state, and has also been reported for bovRho (Kono et al. 2008).

2.3 Action spectra of photoactivated cyclases

We next tested our illumination plate with photoactivated cyclases for direct manipulation of intracellular cyclic mononucleotide signaling (Figure 4A). The soluble photo-activated adenylyl cyclase bPAC from the bacterium *Beggiatoa* sp. is a well-established optogenetic tool with a blue light sensor using flavin adenine dinucleotide (BLUF) as activator domain (Ryu et al. 2010; Stierl et al. 2011; Tan et al. 2022). Purified bPAC has a peak absorbance at about 440 nm (dark adapted state), while the signaling state has a maximum at 455 nm, with the dark state recovering within 19 s (Lindner et al. 2017; Stierl et al. 2011). Our action spectra indicate a maximum between 440 and 460 nm (Figure 4B). To benchmark the spectral resolution of the RainbowCap, we compared the bPAC wildtype (bPAC-wt) with the S27A mutant of bPAC, which shows a 10–15 nm red shift in the absorption spectrum of the purified protein (Stierl et al.
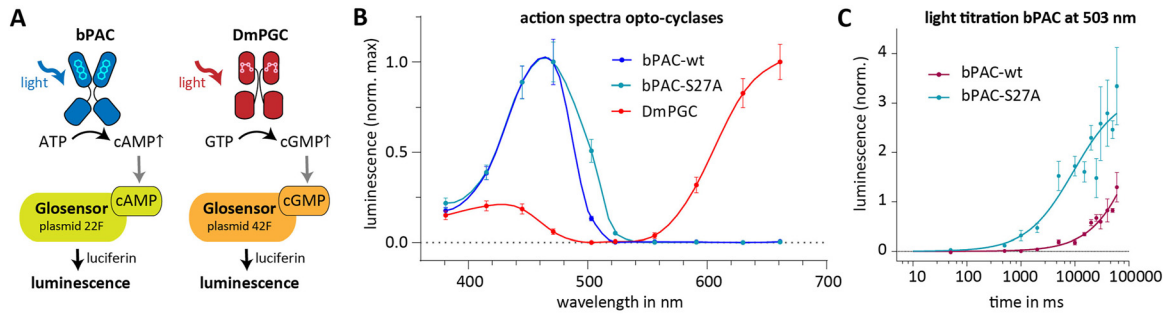
Figure 4: Action spectra of photoactivated cyclases. (A) bPAC is a blue light-activated adenylyl cyclase that uses flavin as chromophore. DmPGC is a red light-activated guanylyl cyclase with biliverdin as chromophore. Changes in cAMP or cGMP levels are reflected by luminescence output generated by the GloSensor plasmids 22F or 42F, respectively. (B) Action spectra of bPAC-wt, the mutant bPAC-S27A, and DmPGC determined after 15 s illumination. Both bPAC-wt and bPAC-S27A are most effectively activated at 460 nm, but the mutant also shows a 10 nm red-shifted shoulder. DmPGC is strongly activated by light >630 nm. Illuminations were performed in the presence of luciferin and plates were used repeatedly for light titration experiments. (C) Log-scale plot of light titration experiments at 503 nm. At this wavelength, the bPAC-S27A mutant has a higher light sensitivity than the wt. All data points in B and C are indicated as mean ± SEM (*n*-values are listed in Supplementary Figure 10). Curve fits are performed with spline fit in B and with the dose-response equation in C.
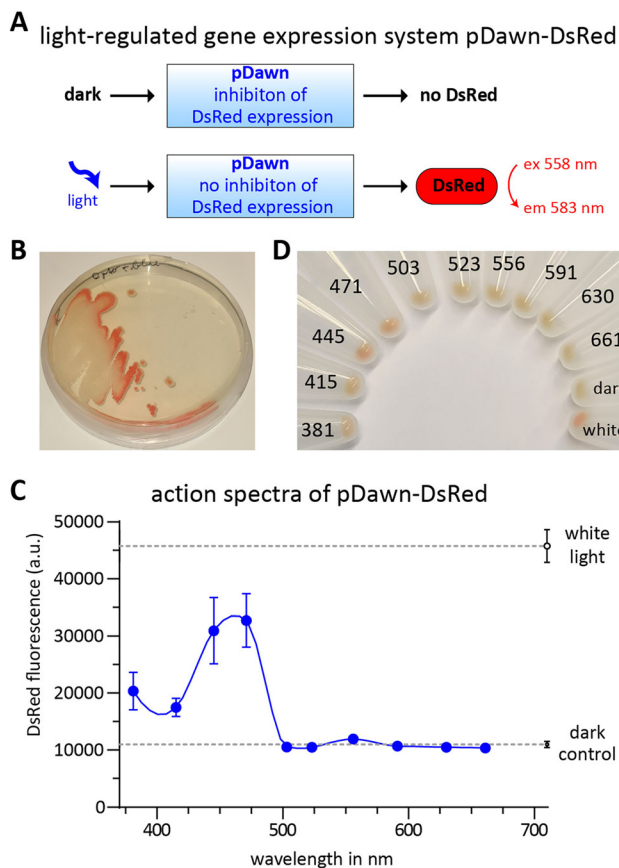

Figure 5: Evaluation of the RainbowCap for the light-regulated gene expression system pDawn-DsRed. (A) Simplified schematic of the expression system. Blue light initiates the expression of the fluorescent reporter protein DsRed (see reference and text for details). (B) Agar plate with transformed *E. coli* bacteria. Partial exposure of the agar plate with blue light-activated the gene expression of DsRed. (C) Action spectra of pDawn determined with the RainbowCap. The fluorescence of DsRed was plotted against the illumination wavelength of each sample (mean ± SEM, *n* = 4). (D) DsRed is visible in bacterial pellets from blue light samples and the white light control.

2014). Indeed, the action spectra indicated an increased sensitivity at 503 nm of the bPAC-S27A mutant (Figure 4B), but we could not observe a bathochromic shift of the peak activity. However, light titration at 503 nm showed that the difference between wt and S27A relate to a higher light sensitivity of the mutant at longer wavelengths (Figure 4C, Supplementary Figure 11C–G).

The red light-activated guanylyl cyclase DmPGC is a novel engineered optogenetic tool that allows increasing cGMP levels upon illumination. DmPGC is a recombinant photoreceptor that harnesses biliverdin as chromophore, and is comprised of the photosensory core module from the *Deinococcus maricopensis* bacterial phytochrome and the cyclase effector module Cya2 of *Synechocystis* sp. PCC6803 (Xu et al. 2024). As expected for a biliverdin-dependent photoreceptor, DmPGC showed peak activity at >660 nm in our experiments (Figure 4B). Of note, bacterial phytochromes are excited by red/far-red light and the actual maximum is probably outside of the range of our current RainbowCap (Tan et al. 2022). The moderate activation of DmPGC at 420 nm owes to the Soret band typical for tetrapyrroles such as biliverdin (Xu et al. 2024).

2.4 Action spectra of an optogenetic gene expression system

As a further application test, we applied our illumination plate on the engineered light-regulated gene expression system pDawn-DsRed, shown in Figure 5A (Ohlendorf et al. 2012). The pDawn system controls gene expression by a two-step mechanism: The engineered photoreceptor (YF1/FixJ) of pDawn is active in the dark state and drives the expression of

a repressor protein (Moglich et al. 2009; Ohlendorf et al. 2012). This repressor protein in turn inhibits the expression of DsRed. Therefore, illumination of the photoreceptors leads to expression of DsRed (Figure 5B). As bPAC, the YF1/FixJ photoreceptor uses a flavin nucleotide as blue light sensitive chromophore. For determining the exact action spectrum of pDawn-DsRed, *E. coli* bacteria transformed with pDawn-DsRed were cultured to stationary phase and plated in black 96-well microplates with transparent bottoms. Plates were illuminated overnight using the RainbowCap. On the following day, we measured DsRed fluorescence in the wells and calculated the resulting action spectrum, which corresponds to that of flavin-based photoreceptors (Figure 5C). For visualization, bacteria samples were then pooled and centrifuged. Expression of DsRed can be seen in pellets from cultures illuminated with 445 and 471 nm, and in the white light control (Figure 5D).

3 Discussion

The RainbowCap offers simultaneous spectral illumination of microplates, with considerable scope for spectral screening and investigation of new natural and recombinant optogenetic proteins, but also with potential applications in other areas of photobiology research. Earlier devices for programmable illumination of microplates resorted to a limited number of LEDs and did not incorporate optical filters, or were optimized for spectroscopy (Baillargeon et al. 2019; Benman et al. 2023; Bugaj and Lim 2019; Gerhardt et al. 2016; Hohener et al. 2022; Kagel et al. 2019; Kumar and Khammash 2022; Qi et al. 2018; Richter et al. 2015). Consequently, the RainbowCap offers significant advantages compared to these devices when it comes to the determination of action spectra. The combination of the Rainbow-Cap with plate readers offers a high-throughput approach compared to electrophysiological methods for determining action spectra. Our strategy is also compatible with light sensitive cells in suspension, whereas electrophysiological methods are limited to adherent cells. We have shown this for *E. coli* cultures, but the RainbowCap could also enable optogenetic experiments on non-adherent eukaryotic cells such as immune cells in the future (Malogolovkin et al. 2022; Nguyen et al. 2021).

We validated the RainbowCap using optogenetic proteins with different functions and chromophores. We determined a peak activity at 485 ± 5 nm for JellyOp and at 483 ± 5 nm for bovRho after supplementation of cells with all-*trans* retinal (Figure 3G). These λ_{max}-values likely correspond to an isomer mixture as confirmed in our experiments with purified retinal isomers (Figure 3H and I).

For the different isomers, we determined peak activities of JellyOp at 469 ± 10 nm, 488 ± 10 nm, and 460 ± 8 nm in presence of 9-*cis*, 11-*cis* and 13-*cis* retinal, respectively. The difference in the peak activity of JellyOp observed in the measurement in presence of 11-*cis* retinal, which is approximately 12 nm different from the value reported by Gerrard et al. (2018), could be attributed to differences in the illumination method and protocol or the implementation of the curve fit. However, the shifts between the isomers are in line with the absorption spectra of bovRho reconstituted with 11-*cis* retinal (497 nm), 9-*cis* (486 nm), and 13-*cis* (467 nm) (Araujo et al. 2014). However, it should also be noted that the absorption spectra of purified protein and the action spectra in biological systems can be different (Coohill 1991; Haxo and Blinks 1950). Furthermore, all our rhodopsin spectra result from stationary illuminations that start from the dark-adapted state and sequential absorption of multiple photons causing secondary photoreactions cannot be excluded.

In addition, we investigated the action spectrum of the red light-activated guanylyl cyclase DmPGC and found strongest activation at a wavelength >630 nm (Figure 4B). This is of particular interest for *in vivo* optogenetic applications, as red light has superior tissue penetration, facilitating the activation of optogenetic proteins at low light intensities. It may also be possible to combine DmPGC with sensors or actuators sensitive in the 460–560 nm light range with minimal optical crosstalk.

A potential caveat of using the GloSensor as readout is that the luminescence itself could lead to the activation of optogenetic proteins. However, we could not find evidence for such effects in our spectral experiments. Optogenetic proteins that are excited by luminescence exist ("luminopsins"), but in these cases the luciferase is fused directly to the optogenetic protein or both components are in immediate vicinity at the synapse (Gomez-Ramirez et al. 2020; Prakash et al. 2022; Tan et al. 2022; Tung et al. 2015).

While the current illumination system is the result of different testing strategies and incremental improvements (see Supplementary Figure 12), we also see potential for future improvements. One important aspect is to further prevent light contamination in and around the illumination setup, especially for long time illumination experiments and highly light sensitive proteins with slow deactivation kinetics. In this context, we would like to emphasize the light spillover at the bottom and around the edges of white microplates (see Supplementary Figure 13). In addition, the RainbowCap could also be adapted for illumination from below, which would make it possible to achieve sterile conditions during long-term experiments. The integration of temperature control and other environmental factors such

as humidity is also conceivable. In the long term, a better spectral resolution of the action spectra and an extension with LEDs to the near infrared range is preferable. In its current version, the RainbowCap is based on standard electronic components that allows for easy replication and can be readily integrated with any plate reader without any hardware modification. Miniaturization of the components would be advantageous, allowing electronic control of each LED to allow eight different simultaneous illumination times or even adaption to 384-well microplates. Especially for high-throughput screening with multiple microplates, it will be helpful to integrate the illumination plate into automated plate reader screening systems. A further improvement could be achieved by automated fine adjustment of the LED intensities as recently developed for a microplate illumination device for absorbance and fluorescence readouts (Benman et al. 2023). Finally, simultaneous spectral illumination of the entire microplate within the plate reader would also be ideal, which would permit measurements of shorter-lived light-induced activities (<1 min). Thus, the RainbowCap paves the way for highly parallelized, quantitative spectral characterizations of optogenetic tools and photobiological processes.

4 Materials and methods

4.1 Construction of the RainbowCap

The 3D-printing files for the filter plate, the LED plate and the photodiode adapter were created using the 3D Builder software (Microsoft Corporation). Polyamide laser sintering (PA2200) with black coloration was chosen for printing (Murtfeldt Additive Solutions GmbH, Germany). The holes for the screws were drilled after printing. Both plates were connected after insertion of the optical filters and the assembly of the LEDs and electronics (see Figure 1, Supplementary Figures 1–4). The 11th column was covered with black tape as dark control. Two LEDs of the same color (i.e. four pairs per column, total 44 pairs) were connected with a 500 Ω precision potentiometer (25 turns, WIW3296-y-501, Shaanxi Hongxing Electronic Components) in row with a bipolar transistor BC337-40 (NPN BC337-40, Diotec Semiconductor) and a 1 kΩ fixed resistor (WIW3296-w-102, Shaanxi Hongxing Electronic Components). These LED-pairs were connected to the respective voltage converter (voltage step-down modules, BN 2134134, Maker Factory) on an additional supply board with six different voltages (4.22, 2.77, 2.50, 2.70, 2.48 and 3.30 V). For example, the UV and blue LEDs run at 4.22 V, while the yellow and red LEDs were supplied with 2.70 or 2.48 V. The required voltages were determined beforehand (see next section for calibration of the LEDs). All

voltage converters were operated with a laboratory power supply set to constant 9 V and a maximum of 500 mA (NTP-5531, Manson Engineering Industrial Ltd). In addition, all LED-pairs were connected to a microcontroller (Arduino Board Mega 2560 Core or Joy-IT Mega 2560 R3). The microcontroller controls all 44 transistors of the illumination plate individually, therefore 44 different illumination protocols (four per wavelength) could be implemented with our circuit. The 3D printing files, circuit plans, and the microprocessor programs (sketches) are publicly available via github (https://github.com/arvogt/RainbowCap-project).

4.2 Validation and calibration of LED-filter pairs

We first measured current-voltage relationships, the respective spectra, and the light intensities for each LED type without optical filters, using an LED-Tester (M087N, KEMO Electronic, Germany) and a spectroradiometer (CSS-45, Gigahertz-Optik GmbH, Germany) (Supplementary Figures 4 and 5). Some diodes of the same manufacturer showed considerable deviations and only comparable LEDs were further used. After all electronic components and LED-filter pairs were installed, we adjusted the voltages for the LEDs to achieve uniform photon flux. For this purpose, we measured light intensities of all LEDs individually and fine-tuned the voltage via the adjustable resistors.

4.3 Molecular biology

Fusion constructs with mScarlet of genes encoding Jelly rhodopsin from *C. rastonii* (JellyOp, UniProtKB B6F0Y5), bovine rhodopsin (bovRho, UniProtKB P02699), bPAC from the bacteria *Beggiatoa sp.* (UniProtKB A7BT71), or DmPGC (deposited at Addgene, #220309) (Xu et al. 2024) were subcloned into the pcDNA3.1 vector. The plasmid for the GsX-assay (Ballister et al. 2018) was obtained from Addgene (G_{st}-Ser, #109354).

4.4 Cell culture

HEK293TN cells (System Biosciences, SBI) were routinely cultured in DMEM + GlutaMAX medium supplemented with 1 % penicillin/streptomycin, 10 % fetal bovine serum (FCS; all ThermoFisher Scientific), and 1 µM all-*trans* retinal (Sigma-Aldrich). For experiments involving retinal isomers, we established HEK293TN cultures with serum-reduced conditions, as FCS contains undefined amounts of vitamin A. FCS content of the cultures was reduced to 2.5 % in three steps, each one week apart, while replacing FCS with Panexin CD (P04-930500, Pan-

Biotech). Morphology and mitotic rate of HEK293TN cells grown in DMEM with 2.5 % FCS, 7.5 % Panexin CD and 1 % penicillin/streptomycin were indistinguishable from cells grown in 10 % FCS. Cells were seeded into black 96-well microplates with white wells (15,000 cells per well, Porvair Sciences). These microplates were exposed to UV light for 30 min beforehand for sterilization. After 24 h, cells were co-transfected with plasmids encoding the optogenetic proteins, the G_{st}-Ser-protein (if needed), and the plasmid for the luciferase-based cAMP-biosensor (plasmid pGloSensor-22F, Promega) or cGMP-biosensor (plasmid pGloSensor-42F, Promega) using XtremeGENE 9 (Roche Diagnostics) as transfection reagent.

Medium was replaced 24 h after transfection with 80 μl/well of the CO$_2$-independent Leibovitz's L-15 medium (ThermoFisher Scientific), supplemented with 10 % FCS, 1 μM all-*trans* retinal, and antibiotics. Plates were incubated for at least another 12 h at 37 °C in an incubator completely protected from light in metal boxes.

For experiments with specific retinal isomers, the medium was replaced with 60 μl/well of L-15 medium supplemented with 10 % Panexin CD and antibiotics. 1–2 h prior to the measurements, we added 20 μl L15 medium together with the respective isomer to achieve a final concentration of 1 μM retinal per well.

4.5 Retinal purification

The purification of retinal isomers (9-*cis*, 11-*cis*, 13-*cis*) was conducted under dim red light conditions following published protocols (Gundersen 2006; Noll 1996). For purification, the Shimadzu HPLC System consisting of the LC20AR-PUMPE, SPD-M20A-DETECTOR, Valve Unit FCV-20AH2, equipped with the appropriate column (ReproSil 70 Si, 5 μm), was utilized. The purification process began with 30 mg of all-*trans* retinal (Sigma-Aldrich) dissolved in 10 ml of acetonitrile, followed by illumination with bright white light for 25 min on ice. Solvent exchange from acetonitrile to 7 % v/v diethyl ether was carried out using a rotary evaporator, followed by an HPLC run at 1 ml/min with manual sample collection For concentration determination, the solvent was exchanged to ethanol, and concentration was calculated using the following extinction coefficients (9-*cis*: $36,070 \times M^{-1} \times cm^{-1}$; 11-*cis*: $24,900 \times M^{-1} \times cm^{-1}$; 13-*cis*: $35,500 \times M^{-1} \times cm^{-1}$) (Horwitz and Heller 1973). The retinal isomers were aliquoted and stored in light-tight containers at –80 °C until usage.

4.6 Illumination of microplates

Transfected cells were transferred under red darkroom light into a Mithras LB 940 plate reader (Berthold Technologies).

The plates were incubated in the plate reader for at least 30 min to equalize temperature. The instrument temperature was set to 29 °C and all measurements were performed at this temperature. This was a compromise because the reader cannot maintain room temperature in continuous operation, and we wanted to keep the cells vital for hours, but the luminescence is higher at lower temperature. The microplate was taken out of the plate reader for illumination. Handling time was kept as short as possible to prevent temperature artifacts (see Supplementary Figure 7). Great care was taken to protect the samples from light, and only red light or no light (for red light-activated DmPGC) was used for room lighting. Ten microliter luciferin stock solution (solved in L15 medium) was added via injectors to each well (final volume of 90 μl per well with 0.6 mg ml^{-1} sodium D-Luciferin, 2 % v/v, Promega). Luminescence was recorded with an integration time of 0.2 s per well. At the end of the measurements, the adenylyl cyclase activator forskolin to increase cAMP levels (Tocris; final concentration 10 μM) or the nitric oxide (NO) donor sodium nitroprusside to increase cGMP level (Sigma-Aldrich; final concentration 25 μM) were injected via the plate reader as light-independent positive controls.

4.7 Absorbance and fluorescence scan

Luciferin absorption spectrum, fluorescence excitation spectrum (emission at 535 nm) and emission spectrum (excitation at 330 nm) were measured using a Tecan Spark multimode plate reader. Since the spectral properties of luciferin are pH dependent, luciferin was solved in L15 medium with the same supplements as in the GloSensor assay.

4.8 Data analysis

Luminescence values for each well were first normalized to the maximum of the light-independent positive control (10 μM forskolin or 25 μM sodium nitroprusside). The highest value after the illumination was always selected. The evaluation using the integral was not applied because the initial signal increase could not always be fully measured, particularly with the fast JellyOp (Supplementary Figure 6B). For JellyOp and bovine rhodopsin, the resulting normalized data were used directly for the statistical model (see Supplementary Materials). In the case of cyclase DmPGC, the high basal activity of the GloSensor plasmid for cGMP was subtracted for each single well as part of the normalization with sodium nitroprusside. The normalized values of the dark controls were afterwards subtracted from the normalized values of bPAC and DmPGC.

Curve fits for the cyclases are performed with spline fits and with the dose-response equation (y = [activity$_{max}$ × time]/[EC_{50} + time]). Numbers of replicates (n-numbers) are stated in Supplementary Figure 10. GraphPad Prism 9 software was used for analysis and graphical presentation.

4.9 Bayesian framework for determining rhodopsin action spectra

We implemented a Bayesian modeling approach to analyze the activity measurements (Gabry et al. 2019). The detailed description of the method is provided as Supplementary Materials. Functional activity of light titrations was used to estimate the normalized spectral activity and activity peak wavelength. As a basis for the estimation, we used the template for visual pigment absorption spectra by Govardovskii et al. (2000). However, this template only works for values normalized to the maximum and does not account for inter-experiment variability. We modified the approach to fit normalized spectral densities of opsins by fitting α- and β-bands scaled by the activity amplitude. The amplitude was estimated depending on the illumination time using a dosage-saturation curve with additional estimation of dark activity. Further we allowed the model to estimate adjustments to the previously published fixed parameters accommodating shape differences between the Govardovskii template for absorbance spectral densities and action spectra. Finally, we implemented a hierarchical model to account for inter-experimental variance using *Stan* (version 2.34.1) (Carpenter et al. 2017; Stan Development Team 2023) via *cmdstanr* (version 0.7.1) (Gabry et al. 2023). The fits are presented as the estimated marginal mean (fits for experiments averaged over construct) and the corresponding 95 % highest density interval using *bayestestR* (Makowski et al. 2019). The model and analysis are provided at https://github.com/danielparthier/Vogt-et-al-2024.

4.10 Optogenetic gene expression in *E. coli*

All experiments were performed in the dark or, if necessary, under red light. Single colonies of a standard Agar-plate with *E. coli* transfected with the pDawn-DsRed plasmid were grown in 100 ml overnight cultures (37 °C, shaking). Cultures were cultivated to maximum density. Two hundred microliter cell suspension/well was dispensed into each well of a black microplate with clear flat bottom (Greiner, 655090). The microplate was then illuminated overnight for 16 h at room temperature using the RainbowCap. The illumination protocol consisted of 15 min of light alternating with 15 min of darkness. Fluorescence was then measured in the wells using a Tecan Spark multimode plate reader in bottom reading mode (excitation 530 ± 20 nm, emission 610 ± 20 nm). Cells were briefly vortexed by the reader before fluorescence was measured.

References

Araujo, N.A., Sanz-Rodriguez, C.E., and Bubis, J. (2014). Binding of rhodopsin and rhodopsin analogues to transducin, rhodopsin kinase and arrestin-1. *World J. Biol. Chem.* 5: 254–268.

Bailes, H.J. and Lucas, R.J. (2013). Human melanopsin forms a pigment maximally sensitive to blue light (lambdamax approximately 479 nm) supporting activation of G(q/11) and G(i/o) signalling cascades. *Proc. Biol. Sci.* 280: 20122987.

Bailes, H.J., Zhuang, L.Y., and Lucas, R.J. (2012). Reproducible and sustained regulation of Galphas signalling using a metazoan opsin as an optogenetic tool. *PLoS One* 7: e30774.

Baillargeon, P., Coss-Flores, K., Singhera, F., Shumate, J., Williams, H., DeLuca, L., Spicer, T.P., and Scampavia, L. (2019). Design of microplate-compatible illumination panels for a semiautomated benchtop pipetting system. *SLAS Technol.* 24: 399–407.

Ballister, E.R., Rodgers, J., Martial, F., and Lucas, R.J. (2018). A live cell assay of GPCR coupling allows identification of optogenetic tools for controlling Go and Gi signaling. *BMC Biol.* 16: 10.

Benman, W., Datta, S., Gonzalez-Martinez, D., Lee, G., Hooper, J., Qian, G., Leavitt, G., Salloum, L., Ho, G., Mhatre, S., et al. (2023). High-throughput feedback-enabled optogenetic stimulation and spectroscopy in microwell plates. *Commun. Biol.* 6: 1192.

Bernal Sierra, Y.A., Rost, B.R., Pofahl, M., Fernandes, A.M., Kopton, R.A., Moser, S., Holtkamp, D., Masala, N., Beed, P., Tukker, J.J., et al. (2018). Potassium channel-based optogenetic silencing. *Nat. Commun.* 9: 4611.

Binkowski, B.F., Butler, B.L., Stecha, P.F., Eggers, C.T., Otto, P., Zimmerman, K., Vidugiris, G., Wood, M.G., Encell, L.P., Fan, F., et al. (2011). A luminescent biosensor with increased dynamic range for intracellular cAMP. *ACS Chem. Biol.* 6: 1193–1197.

Brueggemann, L.I. and Sullivan, J.M. (2002). HEK293S cells have functional retinoid processing machinery. *J. Gen. Physiol.* 119: 593–612.

Bugaj, L.J. and Lim, W.A. (2019). High-throughput multicolor optogenetics in microwell plates. *Nat. Protoc.* 14: 2205–2228.

Carpenter, B., Gelman, A., Hoffman, M.D., Lee, D., Goodrich, B., Betancourt, M., Brubaker, M., Guo, J., Li, P., and Riddell, A. (2017). Stan: a probabilistic programming language. *J. Stat. Software* 76: 1–32.

Choe, H.W., Kim, Y.J., Park, J.H., Morizumi, T., Pai, E.F., Krauss, N., Hofmann, K.P., Scheerer, P., and Ernst, O.P. (2011). Crystal structure of metarhodopsin II. *Nature* 471: 651–655.

Chow, B.Y., Han, X., Dobry, A.S., Qian, X., Chuong, A.S., Li, M., Henninger, M.A., Belfort, G.M., Lin, Y., Monahan, P.E., et al. (2010). High-performance genetically targetable optical neural silencing by light-driven proton pumps. *Nature* 463: 98–102.

Coohill, T.P. (1991). Action spectra again. *Photochem. Photobiol.* 54: 859–870.

Deval, P. and Singh, A.K. (1988). Photoisomerization of all-trans-retinal in organic-solvents and organized media. *J. Photochem. Photobiol. A* 42: 329–336.

Emiliani, V., Entcheva, E., Hedrich, R., Hegemann, P., Konrad, K.R., Lüscher, C., Mahn, M., Pan, Z.-H., Sims, R.R., Vierock, J., et al. (2022). Optogenetics for light control of biological systems. *Nat. Rev. Methods Prim.* 2: 55.

Gabry, J., Češnovar, R., and Johnson, A. (2023). cmdstanr: R interface to 'CmdStan', Available at: https://mc-stan.org/cmdstanr/, https://discourse.mc-stan.org.

Gabry, J., Simpson, D., Vehtari, A., Betancourt, M., and Gelman, A. (2019). Visualization in Bayesian workflow. *J. Roy. Stat. Soc. Ser. A: Stat. Soc.* 182: 389–402.

Gao, S., Nagpal, J., Schneider, M.W., Kozjak-Pavlovic, V., Nagel, G., and Gottschalk, A. (2015). Optogenetic manipulation of cGMP in cells and animals by the tightly light-regulated guanylyl-cyclase opsin CyclOp. *Nat. Commun.* 6: 8046.

Gerhardt, K.P., Olson, E.J., Castillo-Hair, S.M., Hartsough, L.A., Landry, B.P., Ekness, F., Yokoo, R., Gomez, E.J., Ramakrishnan, P., Suh, J., et al. (2016). An open-hardware platform for optogenetics and photobiology. *Sci. Rep.* 6: 35363.

Gerrard, E., Mutt, E., Nagata, T., Koyanagi, M., Flock, T., Lesca, E., Schertler, G.F.X., Terakita, A., Deupi, X., and Lucas, R.J. (2018). Convergent evolution of tertiary structure in rhodopsin visual proteins from vertebrates and box jellyfish. *Proc. Natl. Acad. Sci. U.S.A.* 115: 6201–6206.

Gomez-Ramirez, M., More, A.I., Friedman, N.G., Hochgeschwender, U., and Moore, C.I. (2020). The BioLuminescent-OptoGenetic *in vivo* response to coelenterazine is proportional, sensitive, and specific in neocortex. *J. Neurosci. Res.* 98: 471–480.

Govardovskii, V.I., Fyhrquist, N., Reuter, T., Kuzmin, D.G., and Donner, K. (2000). In search of the visual pigment template. *Vis. Neurosci.* 17: 509–528.

Gundersen, T.E. (2006). Methods for detecting and identifying retinoids in tissue. *J. Neurobiol.* 66: 631–644.

Haxo, F.T. and Blinks, L.R. (1950). Photosynthetic action spectra of marine algae. *J. Gen. Physiol.* 33: 389–422.

Henss, T., Nagpal, J., Gao, S., Scheib, U., Pieragnolo, A., Hirschhauser, A., Schneider-Warme, F., Hegemann, P., Nagel, G., and Gottschalk, A. (2022). Optogenetic tools for manipulation of cyclic nucleotides functionally coupled to cyclic nucleotide-gated channels. *Br. J. Pharmacol.* 179: 2519–2537.

Hofmann, K.P., Scheerer, P., Hildebrand, P.W., Choe, H.W., Park, J.H., Heck, M., and Ernst, O.P. (2009). A G protein-coupled receptor at work: the rhodopsin model. *Trends Biochem. Sci.* 34: 540–552.

Hohener, T.C., Landolt, A.E., Dessauges, C., Hinderling, L., Gagliardi, P.A., and Pertz, O. (2022). LITOS: a versatile LED illumination tool for optogenetic stimulation. *Sci. Rep.* 12: 13139.

Horwitz, J. and Heller, J. (1973). Interactions of all-trans, 9-11-and 13-cis-retinal, all-trans-retinyl acetate, and retinoic acid with human retinol-binding protein and prealbumin. *J. Biol. Chem.* 248: 6317–6324.

Kagel, H., Jacobs, H., Bier, F.F., Glökler, J., and Frohme, M. (2019). A novel microtiter plate format high power open source LED array. *Photonics* 6: 17.

Kanaho, Y., Tsai, S.C., Adamik, R., Hewlett, E.L., Moss, J., and Vaughan, M. (1984). Rhodopsin-Enhanced Gtpase activity of the inhibitory Gtp-binding protein of adenylate-cyclase. *J. Biol. Chem.* 259: 7378–7381.

Khorana, H.G., Knox, B.E., Nasi, E., Swanson, R., and Thompson, D.A. (1988). Expression of a bovine rhodopsin gene in Xenopus oocytes: demonstration of light-dependent ionic currents. *Proc. Natl. Acad. Sci. U.S.A.* 85: 7917–7921.

Klapoetke, N.C., Murata, Y., Kim, S.S., Pulver, S.R., Birdsey-Benson, A., Cho, Y.K., Morimoto, T.K., Chuong, A.S., Carpenter, E.J., Tian, Z., et al. (2014). Independent optical excitation of distinct neural populations. *Nat. Methods* 11: 338–346.

Kleinlogel, S., Vogl, C., Jeschke, M., Neef, J., and Moser, T. (2020). Emerging approaches for restoration of hearing and vision. *Physiol. Rev.* 100: 1467–1525.

Kono, M., Goletz, P.W., and Crouch, R.K. (2008). 11-cis- and all-trans-retinols can activate rod opsin: rational design of the visual cycle. *Biochemistry* 47: 7567–7571.

Koyanagi, M., Takano, K., Tsukamoto, H., Ohtsu, K., Tokunaga, F., and Terakita, A. (2008). Jellyfish vision starts with cAMP signaling mediated by opsin-G(s) cascade. *Proc. Natl. Acad. Sci. U.S.A.* 105: 15576–15580.

Kumar, S. and Khammash, M. (2022). Platforms for optogenetic stimulation and feedback control. *Front. Bioeng. Biotechnol.* 10: 918917.

Li, X., Gutierrez, D.V., Hanson, M.G., Han, J., Mark, M.D., Chiel, H., Hegemann, P., Landmesser, L.T., and Herlitze, S. (2005). Fast noninvasive activation and inhibition of neural and network activity by vertebrate rhodopsin and green algae channelrhodopsin. *Proc. Natl. Acad. Sci. U.S.A.* 102: 17816–17821.

Lindner, R., Hartmann, E., Tarnawski, M., Winkler, A., Frey, D., Reinstein, J., Meinhart, A., and Schlichting, I. (2017). Photoactivation mechanism of a bacterial light-regulated adenylyl cyclase. *J. Mol. Biol.* 429: 1336–1351.

Mahn, M., Saraf-Sinik, I., Patil, P., Pulin, M., Bitton, E., Karalis, N., Bruentgens, F., Palgi, S., Gat, A., Dine, J., et al. (2021). Efficient optogenetic silencing of neurotransmitter release with a mosquito rhodopsin. *Neuron* 109: 1621–1635.e1628.

Makowka, P., Bruegmann, T., Dusend, V., Malan, D., Beiert, T., Hesse, M., Fleischmann, B.K., and Sasse, P. (2019). Optogenetic stimulation of G(s)-signaling in the heart with high spatio-temporal precision. *Nat. Commun.* 10: 1281.

Makowski, D., Ben-Shachar, M.S., and Lüdecke, D. (2019). bayestestR: describing effects and their uncertainty, existence and significance within the Bayesian framework. *J. Open Source Softw.* 4: 1541.

Malogolovkin, A., Egorov, A.D., Karabelsky, A., Ivanov, R.A., and Verkhusha, V.V. (2022). Optogenetic technologies in translational cancer research. *Biotechnol. Adv.* 60: 108005.

Masseck, O.A., Spoida, K., Dalkara, D., Maejima, T., Rubelowski, J.M., Wallhorn, L., Deneris, E.S., and Herlitze, S. (2014). Vertebrate cone opsins enable sustained and highly sensitive rapid control of Gi/o signaling in anxiety circuitry. *Neuron* 81: 1263–1273.

Moglich, A., Ayers, R.A., and Moffat, K. (2009). Design and signaling mechanism of light-regulated histidine kinases. *J. Mol. Biol.* 385: 1433–1444.

Muhlhauser, W.W., Fischer, A., Weber, W., and Radziwill, G. (2017). Optogenetics – bringing light into the darkness of mammalian signal transduction. *Biochim. Biophys. Acta Mol. Cell Res.* 1864: 280–292.

Murphy, C., Matikainen-Ankney, B., Chang, Y.H., Copits, B., and Creed, M.C. (2021). Optogenetically-inspired neuromodulation: translating basic discoveries into therapeutic strategies. *Int. Rev. Neurobiol.* 159: 187–219.

Nguyen, N.T., Huang, K., Zeng, H., Jing, J., Wang, R., Fang, S., Chen, J., Liu, X., Huang, Z., You, M.J., et al. (2021). Nano-optogenetic engineering of CAR T cells for precision immunotherapy with enhanced safety. *Nat. Nanotechnol.* 16: 1424–1434.

Noll, G.N. (1996). High-performance liquid chromatographic analysis of retinal and retinol isomers. *J. Chromatogr. A* 721: 247–259.

Ohlendorf, R., Vidavski, R.R., Eldar, A., Moffat, K., and Moglich, A. (2012). From dusk till dawn: one-plasmid systems for light-regulated gene expression. *J. Mol. Biol.* 416: 534–542.

Palczewski, K., Kumasaka, T., Hori, T., Behnke, C.A., Motoshima, H., Fox, B.A., Le Trong, I., Teller, D.C., Okada, T., Stenkamp, R.E., et al. (2000). Crystal structure of rhodopsin: a G protein-coupled receptor. *Science* 289: 739–745.

Park, J.H., Scheerer, P., Hofmann, K.P., Choe, H.W., and Ernst, O.P. (2008). Crystal structure of the ligand-free G-protein-coupled receptor opsin. *Nature* 454: 183–187.

Prakash, M., Murphy, J., St Laurent, R., Friedman, N., Crespo, E.L., Bjorefeldt, A., Pal, A., Bhagat, Y., Kauer, J.A., Shaner, N.C., et al. (2022). Selective control of synaptically-connected circuit elements by all-optical synapses. *Commun. Biol.* 5: 33.

Qi, Y., Chen, J., Liu, X., Zhou, X., Fan, J., Shentu, P., Idevall-Hagren, O., and Xu, Y. (2018). Development of a wireless-controlled LED array for the tunable optogenetic control of cellular activities. *Engineering* 4: 745–747.

Richter, F., Scheib, U.S., Mehlhorn, J., Schubert, R., Wietek, J., Gernetzki, O., Hegemann, P., Mathes, T., and Moglich, A. (2015). Upgrading a microplate reader for photobiology and all-optical experiments. *Photochem. Photobiol. Sci.* 14: 270–279.

Ryu, M.H., Moskvin, O.V., Siltberg-Liberles, J., and Gomelsky, M. (2010). Natural and engineered photoactivated nucleotidyl cyclases for optogenetic applications. *J. Biol. Chem.* 285: 41501–41508.

Sahel, J.A., Boulanger-Scemama, E., Pagot, C., Arleo, A., Galluppi, F., Martel, J.N., Esposti, S.D., Delaux, A., de Saint Aubert, J.B., de Montleau, C., et al. (2021). Partial recovery of visual function in a blind patient after optogenetic therapy. *Nat. Med.* 27: 1223–1229.

Scheerer, P., Park, J.H., Hildebrand, P.W., Kim, Y.J., Krauss, N., Choe, H.W., Hofmann, K.P., and Ernst, O.P. (2008). Crystal structure of opsin in its G-protein-interacting conformation. *Nature* 455: 497–502.

Scheib, U., Stehfest, K., Gee, C.E., Korschen, H.G., Fudim, R., Oertner, T.G., and Hegemann, P. (2015). The rhodopsin-guanylyl cyclase of the aquatic fungus Blastocladiella emersonii enables fast optical control of cGMP signaling. *Sci. Signal.* 8: rs8.

Spangler, S.M. and Bruchas, M.R. (2017). Optogenetic approaches for dissecting neuromodulation and GPCR signaling in neural circuits. *Curr. Opin. Pharmacol.* 32: 56–70.

Spoida, K., Eickelbeck, D., Karapinar, R., Eckhardt, T., Mark, M.D., Jancke, D., Ehinger, B.V., Konig, P., Dalkara, D., Herlitze, S., et al. (2016). Melanopsin variants as intrinsic optogenetic on and off switches for transient versus sustained activation of G protein pathways. *Curr. Biol.* 26: 1206–1212.

Stan Development Team. (2023). Stan modeling language users guide and reference manual, Available at: https://mc-stan.org.

Stierl, M., Penzkofer, A., Kennis, J.T., Hegemann, P., and Mathes, T. (2014). Key residues for the light regulation of the blue light-activated adenylyl cyclase from Beggiatoa sp. *Biochemistry* 53: 5121–5130.

Stierl, M., Stumpf, P., Udwari, D., Gueta, R., Hagedorn, R., Losi, A., Gartner, W., Petereit, L., Efetova, M., Schwarzel, M., et al. (2011). Light modulation of cellular cAMP by a small bacterial photoactivated adenylyl cyclase, bPAC, of the soil bacterium Beggiatoa. *J. Biol. Chem.* 286: 1181–1188.

Sugiura, M., Tsunoda, S.P., Hibi, M., and Kandori, H. (2020). Molecular properties of new enzyme rhodopsins with phosphodiesterase activity. *ACS Omega* 5: 10602–10609.

Tan, P., He, L., Huang, Y., and Zhou, Y. (2022). Optophysiology: illuminating cell physiology with optogenetics. *Physiol. Rev.* 102: 1263–1325.

Terakita, A., Yamashita, T., Nimbari, N., Kojima, D., and Shichida, Y. (2002). Functional interaction between bovine rhodopsin and G protein transducin. *J. Biol. Chem.* 277: 40–46.

Tung, J.K., Gutekunst, C.A., and Gross, R.E. (2015). Inhibitory luminopsins: genetically-encoded bioluminescent opsins for versatile, scalable, and hardware-independent optogenetic inhibition. *Sci. Rep.* 5: 14366.

Xu, Q., Vogt, A., Frechen, F., Yi, C., Kucukerden, M., Ngum, N., Sitja-Roqueta, L., Greiner, A., Parri, R., Masana, M., et al. (2024). Engineering bacteriophytochrome-coupled photoactivated adenylyl cyclases for enhanced optogenetic cAMP modulation. *J. Mol. Biol.* 436: 168257.

Yoshida, K., Tsunoda, S.P., Brown, L.S., and Kandori, H. (2017). A unique choanoflagellate enzyme rhodopsin exhibits light-dependent cyclic nucleotide phosphodiesterase activity. *J. Biol. Chem.* 292: 7531–7541.